

# Two-dimensional fractional discrete NLS equations: dispersion relations, rogue waves, fundamental and vortex solitons

Ming Zhong<sup>1,2</sup>, Boris A. Malomed<sup>3,4</sup>, Jin Song<sup>1,2</sup>, Zhenya Yan<sup>1,2,\*</sup>

<sup>1</sup>*KLMM, Academy of Mathematics and Systems Science, Chinese Academy of Sciences, Beijing 100190, China*

<sup>2</sup>*School of Mathematical Sciences, University of Chinese Academy of Sciences, Beijing 100049, China*

<sup>3</sup>*Department of Physical Electronics, School of Electrical Engineering, Faculty of Engineering, Tel Aviv University, Tel Aviv 69978, Israel*

<sup>4</sup>*Instituto de Alta Investigación, Universidad de Tarapacá, Casilla 7D, Arica, Chile*

**Abstract** We introduce physically relevant new models of two-dimensional (2D) fractional lattice media accounting for the interplay of fractional intersite coupling and onsite self-focusing. Our approach features novel discrete fractional operators based on an appropriately modified definition of the continuous Riesz fractional derivative. The model of the 2D isotropic lattice employs the discrete fractional Laplacian, whereas the 2D anisotropic system incorporates discrete fractional derivatives acting independently along orthogonal directions with different Lévy indices (LIs). We derive exact linear dispersion relations (DRs), and identify spectral bands that permit linear modes to exist, finding them to be similar to their continuous counterparts, apart from differences in the wavenumber range. Additionally, the modulational instability in the discrete models is studied in detail, and, akin to the linear DRs, it is found to align with the situation in continuous models. This consistency highlights the nature of our newly defined discrete fractional derivatives. Furthermore, using Gaussian inputs, we produce a variety of rogue-wave structures. By means of numerical methods, we systematically construct families of 2D fundamental and vortex solitons, and examine their stability. Fundamental solitons maintain the stability due to the discrete nature of the interactions, preventing the onset of the critical and supercritical collapse. On the other hand, vortex solitons are unstable in the isotropic lattice model. However, the anisotropic one – in particular, its symmetric version with equal LIs acting in both directions – maintains stable vortex solitons with winding numbers  $S = 1$  and  $S = 3$ . The detailed results stress the robustness of the newly defined discrete fractional Laplacian in supporting well-defined soliton modes in the 2D lattice media.

**KEYWORDS** 2D fractional discrete nonlinear equations, discrete fractional Laplacian, modulation instability, rogue waves, fundamental and vortex solitons, stability

## 1 Introduction

In the course of the last thirty years, the fractional calculus has found diverse realizations in physics [1–3], including non-Gaussian stochasticity [4–7], quantum mechanics [8–13], optics [14–20], control theory [21], Bose-Einstein condensates [22], charge transfer in solids [23], etc. Fractional derivatives were first introduced as an abstract mathematical concept [24–27], including definitions such as the Riemann-Liouville and Caputo fractional derivatives [28,29]. The latter one, with a non-integer order  $\alpha$ , is defined as

$$D_x^\alpha u(x) = \frac{1}{\Gamma(1 - \{\alpha\})} \int_0^x \frac{u^{(n)}(s)}{(x-s)^{\{\alpha\}}} ds, \quad (1)$$

---

\* Corresponding author at: KLMM, Academy of Mathematics and Systems Science, Chinese Academy of Sciences, Beijing 100190, China. *Email address:* zyyan@mmsrc.iss.ac.cn (Corresponding author)

where  $n \equiv [\alpha] + 1$  with  $[\alpha]$  and  $\{\alpha\} \equiv \alpha - [\alpha]$  being the integer and fractional parts of  $\alpha$ , respectively,  $\Gamma(\cdot)$  is the Euler's Gamma-function, and  $u^{(n)}(x) = d^n u(x)/dx^n$  denotes the usual derivative of integer-order  $n$ .

In physical applications, the relevant definition is a simpler one, *viz.*, the Riesz fractional derivative (RFD) [30], which follows the intuitive idea that the fractional-order differentiation of wave function  $u(x)$  in the coordinate space is represented by the multiplication by a fractional power,  $|k|^\alpha$ , of wavenumber  $k$  in the Fourier space:

$$\left(-\frac{\partial^2}{\partial x^2}\right)^{\alpha/2} u(x) = \frac{1}{2\pi} \int_{-\infty}^{+\infty} dk |k|^\alpha \int_{-\infty}^{+\infty} u(s) e^{ik(x-s)} ds, \quad (2)$$

where real  $\alpha$ , which usually takes values  $1 < \alpha \leq 2$ , is called the Lévy index (LI) [31]. Thus, RFD is not a differential operator, but an integral (alias *pseudo-differential*) one, represented by the continuous Riesz fractional integrals [32]. A well-known example of the implementation of RFD in physics is provided by the Laskin's fractional Schrödinger equation (FSE) for the wave function of a particle whose stochastic motion in the classical regime is performed by random *Lévy flights*, with the average distance from the initial position,  $x = 0$ , growing with time  $t$  as  $|x| \sim t^{1/\alpha}$ , where  $\alpha$  is the same LI (Sometime, the LI  $\alpha$  takes values  $0 < \alpha \leq 2$  [31]). In the scaled form, the respective one- and two-dimensional (1D and 2D) FSEs in the fractional quantum mechanics are [8,9,13],

$$i \frac{\partial u}{\partial t} = \frac{1}{2} \left(-\frac{\partial^2}{\partial x^2}\right)^{\alpha/2} u + V(x)u, \quad (3)$$

$$i \frac{\partial u}{\partial t} = \frac{1}{2} (-\nabla^2)^{\alpha/2} u + V(x,y)u, \quad (4)$$

where  $\nabla^2 = \partial_x^2 + \partial_y^2$  is the Laplacian, and the fractional Laplacian  $(-\nabla^2)^{\alpha/2}$  can also be defined similar to the 1D case (2),  $V(x)$  and  $V(x,y)$  are the respective real trapping potentials. The limit case of  $\alpha = 2$  corresponds to the usual integer-order Schrödinger equations in canonical quantum mechanics.

While fractional quantum mechanics based on Eqs. (3) and (4) has not yet been realized experimentally, it was proposed by Longhi [16] to emulate it in terms of the classical paraxial light propagation in optical cavities, using the commonly known similarity between the quantum-mechanical Schrödinger equation and parabolic evolution equation for the envelope of optical waves. In that context, the action of RFD (2) may be realized by passing the Fourier-decomposed light beam through a properly designed phase plate, while the continuous equation appears as a result of averaging over many cycles of the light circulation in the cavity. In 2023, Liu *et al* [17] reported the first experimental implementation of the fractional group-velocity dispersion (GVD) in fiber lasers modeled by the generalized FSE in the temporal domain,

$$i \frac{\partial u}{\partial z} = \left[ D_\alpha \left(-\frac{\partial^2}{\partial \tau^2}\right)^{\alpha/2} - \sum_{k=2,3,\dots} \frac{\gamma_k}{k!} \left(i \frac{\partial}{\partial \tau}\right)^k \right] u + V(\tau)u, \quad (5)$$

where  $z$  is the propagation distance,  $\tau$  the time variable,  $D_\alpha$  a real fractional-dispersion parameter,  $\gamma_k$  the real  $k$ -th regular GVD parameter, and  $V(\tau)$  an effective potential.

The emulation of FSEs in terms of the cavity optics makes it possible to essentially extend physically relevant model equations. In particular, it is possible to replace the real effective potential, which represents the refractive-index pattern in the cavity, by complex  $\mathcal{PT}$ -symmetric ones [19]. Furthermore, the optical implementation suggests one to add the usual cubic terms which represent the Kerr effect in optical media [33]. The result is the fractional nonlinear Schrödinger (NLS) equations, such as

$$i \frac{\partial u}{\partial t} = \frac{1}{2} (-\nabla^2)^{\alpha/2} u + V(x,y)u + g|u|^2 u \quad (6)$$

in 2D. In this equation, a real nonlinearity coefficient  $g = +1$  and  $-1$  represents, respectively, self-defocusing and focusing effects, and  $V(x, y)$  denotes an external potential, which is a real-valued function or a complex  $\mathcal{PT}$ -symmetric one, subject to constraint  $V(-x, -y) = V^*(x, y)$ , where  $*$  stands for the complex conjugate. Fractional NLS equations with some external potentials or without potential have been the subject of many theoretical works, which have predicted a variety of fractional solitons, vortices, domain walls, and other nonlinear states – see, in particular, original works [10, 34–49] and reviews [50–52]. Solitons in fractional media with the quadratic (second-harmonic-generating) nonlinearity have been predicted too [53].

Theoretical works addressing fractional nonlinear media were extended towards the consideration of their discrete counterparts (alias fractional lattices) [54–59]. In these works, discrete counterparts of the fractional derivatives of the Riemann-Liouville and Caputo types (see Eq. (1)) were introduced, which amount to nonlocal couplings in the underlying lattices. Previously, similar nonlocally coupled lattice dynamical models were introduced in other contexts [60, 61]. However, the above-mentioned physical realizations of fractional media suggest to introduce their discrete counterparts corresponding to the lattice versions of RFD. More recently, with the aid of the newly-defined discrete fractional derivative, a novel 1D model of this type was elaborated for the 1D fractional lattice with the onsite cubic self-focusing nonlinearity [62]. Moreover, families of discrete solitons of the single- and two-site types, produced by the model, were constructed, and their stability and mobility were also explored [62].

Continuous waves (CWs), alias plane waves, which are the simplest relevant solutions of nonlinear wave equations, are characterized by the spatial wavenumber, related to the respective temporal frequency [63–66]. A key feature of CWs in dispersive wave media is their modulation instability (MI, alias the Benjamin-Feir instability [63]), which makes the CWs unstable under certain conditions [66]. In particular, it is well known that both continuous and discrete NLS equations give rise to MI in the case of the self-focusing nonlinearity. MI is a significant topic across many areas, including fluid dynamics [63, 67], nonlinear optics [68, 69], and plasmas [70, 71]. In particular, rogue waves (RWs) are a well-known kind of wave phenomena related to MI, which draws growing interest in various fields, such as nonlinear optics [72, 73], deep ocean [74, 75], superfluids [76], plasma physics [77], Bose-Einstein condensates [78, 79], atmosphere [80], and even financial markets [81, 82]. RWs are large-amplitude spontaneously generated nonlinear waves that appear suddenly and disappear just as quickly [83]. In 1983, the exact first-order RW (alias the Peregrine soliton/rogon) was found by Peregrine as an exact solution of the integrable focusing NLS equation [84]. Then, it was shown that the Peregrine solitons explain diverse numerical and experimental results [85]. In addition to the fact that the continuous nonlinear wave equations produce RWs (see e.g., Refs. [86–90] and references therein), some discrete integrable nonlinear systems also admit RW solutions [91–99]. Recently, RWs were found in the continuous two-Lévy-index fractional Kerr media [47]. However, the study of RWs was not yet developed in detail in terms of fractional discrete non-integrable systems. With regard to the presence of MI in these systems, we here explore RWs as a linear superposition of CWs and Gaussian perturbations with different parameters in the fractional discrete systems.

The general objective of the present work is to extend the formulation and analysis of 1D fractional discrete systems for 2D lattices with the onsite self-focusing nonlinearity. A new straightforward possibility, offered by the consideration of the 2D setting, is to construct 2D vortex solitons, in addition to the fundamental lattice ones. Two different 2D fractional discrete models are introduced in Section 2. One model is isotropic, with the discrete version of the fractional Laplacian, see Eq. (13) below. The other model is, generally speaking, anisotropic, with two quasi-1D discrete fractional derivatives acting separately along the two directions of the underlying lattice, each derivative being defined by its own coefficient and LI value, see Eq. (14) below. A special role is played by the symmetric version of the latter model, with equal coeffi-

cients and LIs of both fractional derivatives. We derive exact linear dispersion relations (DRs) for these 2D fractional lattice models, and compare them with the known result for the classical discrete NLS (DNLS) equation in Section 3. The MI and RW generation are investigated in Section 4, showing similarities to the results for continuous models. Systematically collected results for the structure and stability of 2D lattice solitons of the fundamental and vortex types, produced by means of numerical methods, are reported, respectively, in Sections 5. In particular, the discreteness provides stability of the 2D solitons against the critical and supercritical collapse in the cases of  $LI = 2$  and  $LI < 2$ , respectively. Vortex solitons are unstable in the framework of the isotropic model with the fractional Laplacian, while the model with the independent quasi-1D fractional derivatives produce stable vortex derivatives, with winding numbers (topological charges)  $S = 1$  and  $3$ . The paper is completed by Section 6.

## 2 2D fractional DNLS equations with quasi-Riesz fractional derivatives (RFDs)

### 2.1 Definition of 2D discrete fractional derivatives

A complex function  $u_{n,m} = u(n, m, \cdot)$  of two discrete integer-value coordinates  $(n, m)$  and other variables can be represented by its Fourier transform,  $U_{k_x, k_y} = U(k_x, k_y, \cdot)$ , which is defined in the interval of  $k_x, k_y \in [-\pi, +\pi]$ , as a periodic function of real continuously varying wavenumbers  $(k_x, k_y)$  in the 2D Fourier space. The direct and inverse Fourier relations between  $u_{n,m}$  and  $U_{k_x, k_y}$  take the usual form,

$$\begin{aligned} u_{n,m} &= \frac{1}{4\pi^2} \int_{-\pi}^{+\pi} \int_{-\pi}^{+\pi} e^{i(k_x n + k_y m)} U_{k_x, k_y} dk, \\ U_{k_x, k_y} &= \sum_{n,m=-\infty}^{+\infty} u_{n,m} e^{-i(k_x n + k_y m)}. \end{aligned} \quad (7)$$

Thus, the new discrete counterpart of the 2D RFD (fractional Laplacian),  $(-\hat{\partial}^2/\hat{\partial}n^2 - \hat{\partial}^2/\hat{\partial}m^2)^{\alpha/2}$ , with the LI  $\alpha \in (1, 2]$ , is defined starting from its natural definition in the Fourier space:

$$\begin{aligned} \left\{ \left( -\frac{\hat{\partial}^2}{\hat{\partial}n^2} - \frac{\hat{\partial}^2}{\hat{\partial}m^2} \right)^{\alpha/2} u \right\}_{n,m} &= \frac{1}{4\pi^2} \int_{-\pi}^{+\pi} \int_{-\pi}^{+\pi} e^{i(k_x n + k_y m)} (k_x^2 + k_y^2)^{\alpha/2} dk_x dk_y \sum_{p,q=-\infty}^{+\infty} u_{p,q} e^{-i(k_x p + k_y q)} \\ &= \frac{1}{4\pi^2} \sum_{p,q=-\infty}^{+\infty} u_{p,q} \int_{-\pi}^{+\pi} \int_{-\pi}^{+\pi} \cos(k_x(p-n) + k_y(q-m)) (k_x^2 + k_y^2)^{\alpha/2} dk_x dk_y \\ &\equiv \sum_{l_x, l_y=-\infty}^{+\infty} D_{l_x, l_y}^{(\alpha)} u_{n+l_x, m+l_y}, \end{aligned} \quad (8)$$

where the caret symbol ( $\hat{\cdot}$ ) indicates the discrete character of the operator, notation  $\{\cdot\}_{n,m}$  implies that it is the value of the fractional Laplacian at the site with coordinates  $(n, m)$ , and the coupling coefficients, which are even functions of  $l_{x,y}$ , are defined as

$$D_{l_x, l_y}^{(\alpha)} = \frac{1}{4\pi^2} \int_{-\pi}^{+\pi} \int_{-\pi}^{+\pi} \cos(k_x l_x) \cos(k_y l_y) (k_x^2 + k_y^2)^{\alpha/2} dk_x dk_y. \quad (9)$$

Note that, in the limit of  $\alpha = 2$  (the non-fractional case), coefficients (9) are different from zero only in the vertical and horizontal directions, i.e., for  $l_x = 0$  or  $l_y = 0$ ; for instance,  $D_{l_x \neq 0, l_y = 0}^{(\alpha)} = 2(-1)^{l_x} l_x^{-2}$ , which

exactly coincide with the coupling coefficients in the 1D fractional DNLS equation [62]. In 1D, the limit of RFD corresponding to  $\alpha = 2$  may represent a physical system built as an array of quasi-1D Bose-Einstein condensates (narrow tubes) of dipolar atoms [62]. In 2D, it is possible to consider a similar network of parallel quasi-1D condensates, with the transverse cross section shaped as a square lattice, but this interpretation requires special analysis which will be reported elsewhere.

Similarly, we can also define the RFD of function  $u_{n,m}$  with respect to the single direction in the 2D space,

$$\begin{aligned} \left\{ \left( -\frac{\widehat{\partial}^2}{\widehat{\partial}n^2} \right)^{\alpha/2} u \right\}_{n,m} &= \frac{1}{4\pi^2} \int_{-\pi}^{+\pi} \int_{-\pi}^{+\pi} e^{-i(k_x n + k_y m)} |k_x|^\alpha dk_x dk_y \sum_{p,q=-\infty}^{+\infty} u_{p,q} e^{i(k_x p + k_y q)} \\ &= \frac{1}{4\pi^2} \sum_{p,q=-\infty}^{+\infty} u_{p,q} \int_{-\pi}^{+\pi} \int_{-\pi}^{+\pi} \cos(k_x(p-n) + k_y(q-m)) |k_x|^\alpha dk_x dk_y \\ &\equiv \sum_{l_x, l_y=-\infty}^{+\infty} E_{l_x, l_y}^{(\alpha)} u_{n+l_x, m+l_y}, \end{aligned} \quad (10)$$

where the real coupling coefficients are

$$E_{l_x, l_y}^{(\alpha)} = \begin{cases} 0, & l_y \neq 0, \\ \frac{1}{\pi} \int_0^\pi \cos(k_x l_x) k_x^\alpha dk_x \equiv E_{l_x}^{(\alpha)}, & l_y = 0. \end{cases} \quad (11)$$

In fact, the same operator as given by Eqs. (10) and (11) appears in the respective 1D model:

$$\begin{aligned} \left\{ \left( -\frac{\widehat{\partial}^2}{\widehat{\partial}n^2} \right)^{\alpha/2} u \right\}_{n,m} &= \frac{1}{2\pi} \int_{-\pi}^{+\pi} e^{-ik_x n} |k_x|^\alpha dk_x \sum_{p=-\infty}^{+\infty} u_p e^{ik_x p} \\ &= \frac{1}{2\pi} \sum_{p=-\infty}^{+\infty} u_p \int_{-\pi}^{+\pi} \cos(k_x(p-n)) |k_x|^\alpha dk_x \\ &\equiv \sum_{l_x=-\infty}^{+\infty} E_{l_x}^{(\alpha)} u_{n+l_x, m}, \end{aligned} \quad (12)$$

with the same coupling coefficients  $E_{l_x}^{(\alpha)}$  as defined in Eq. (11) [62].

## 2.2 2D fractional DNLS equations

With these definitions of discrete fractional derivatives given by Eqs. (8) and (10), the 2D isotropic fractional DNLS equation in the dimensionless form is written as (in the optics notation, with the evolution variable defined as the propagation distance  $z$ , cf. Eq. (5))

$$i \frac{du_{n,m}}{dz} = C \left\{ \left( -\frac{\widehat{\partial}^2}{\widehat{\partial}n^2} - \frac{\widehat{\partial}^2}{\widehat{\partial}m^2} \right)^{\alpha/2} u \right\}_{n,m} - g |u_{n,m}|^2 u_{n,m}, \quad (13)$$

Further, the 2D anisotropic fractional DNLS equation, with independent fractional derivatives, characterized by the respective LIs  $\alpha$  and  $\beta$  ( $\alpha, \beta \in (1, 2]$ ), acting in two directions, is introduced as

$$i \frac{du_{n,m}}{dz} = \left\{ \left[ C_\alpha \left( -\frac{\widehat{\partial}^2}{\widehat{\partial}n^2} \right)^{\alpha/2} + C_\beta \left( -\frac{\widehat{\partial}^2}{\widehat{\partial}m^2} \right)^{\beta/2} \right] u \right\}_{n,m} - g |u_{n,m}|^2 u_{n,m}, \quad (14)$$

where the positive parameters  $C, C_\alpha, C_\beta$  are the coefficients of the fractional discrete diffraction, alias the linear coupling strength between adjacent sites of the lattice, and  $g = +1$  and  $-1$  represents, respectively, self-focusing and defocusing effects.

Equations (13) and (14) conserve their Hamiltonians which are, respectively,

$$H_1 = C \sum_{m,n,p,q} D_{n-p,m-q}^{(\alpha)} u_{n,m}^* u_{p,q} - \frac{g}{2} \sum_{m,n} |u_{n,m}|^4, \quad (15)$$

and

$$H_2 = C_\alpha \sum_{n,p,m} E_{n-p}^{(\alpha)} u_{n,m}^* u_{p,m} + C_\beta \sum_{n,m,q} E_{m-q}^{(\beta)} u_{n,m}^* u_{n,q} - \frac{g}{2} \sum_{m,n} |u_{m,n}|^4. \quad (16)$$

We mainly consider the case of  $C_\alpha = C_\beta \equiv C$  in Eq. (14), with the anisotropy primarily represented by the different LIs. Both Eqs. (13) and (14) also conserve the total power (norm), defined by the obvious expression:

$$P = \sum_{m,n} |u_{n,m}|^2. \quad (17)$$

**Remark 1** Note that these fractional DNLS equations given by Eqs. (13) and (14) can also include a real or complex  $\mathcal{PT}$ -symmetric external potential  $V(m, n, z)$ , and the discrete cubic nonlinear term may be replaced by other ones [62, 100, 101], such as the cubic-quintic competing nonlinearity,  $g_1 |u_{n,m}|^2 u_{n,m} + g_2 |u_{n,m}|^4 u_{n,m}$ , the power-law term,  $|u_{n,m}|^{2p} u_{n,m}$ , the saturable one,  $|u_{n,m}|^2 u_{n,m} / (1 + S |u_{n,m}|^2)$ , and etc.. The 2D fractional DNLS equation can also be extended to the coupled cases, for example, the 2D isotropic coupled fractional DNLS equations

$$\begin{aligned} i \frac{du_{n,m}}{dz} &= C \left\{ \left( -\frac{\widehat{\partial}^2}{\partial n^2} - \frac{\widehat{\partial}^2}{\partial m^2} \right)^{\alpha/2} u \right\}_{n,m} + V_1(n, m, z) u_{n,m} - (g_{11} |u_{n,m}|^2 + g_{12} |v_{n,m}|^2) u_{n,m}, \\ i \frac{dv_{n,m}}{dz} &= C \left\{ \left( -\frac{\widehat{\partial}^2}{\partial n^2} - \frac{\widehat{\partial}^2}{\partial m^2} \right)^{\alpha/2} v \right\}_{n,m} + V_2(n, m, z) v_{n,m} - (g_{12} |u_{n,m}|^2 + g_{22} |v_{n,m}|^2) v_{n,m}, \end{aligned} \quad (18)$$

and 2D anisotropic coupled fractional DNLS equations

$$\begin{aligned} i \frac{du_{n,m}}{dz} &= \left\{ \left[ C_\alpha \left( -\frac{\widehat{\partial}^2}{\partial n^2} \right)^{\alpha/2} + C_\beta \left( -\frac{\widehat{\partial}^2}{\partial m^2} \right)^{\beta/2} \right] u \right\}_{n,m} + V_1(n, m, z) u_{n,m} - (g_{11} |u_{n,m}|^2 + g_{12} |v_{n,m}|^2) u_{n,m}, \\ i \frac{dv_{n,m}}{dz} &= \left\{ \left[ C_\alpha \left( -\frac{\widehat{\partial}^2}{\partial n^2} \right)^{\alpha/2} + C_\beta \left( -\frac{\widehat{\partial}^2}{\partial m^2} \right)^{\beta/2} \right] v \right\}_{n,m} + V_2(n, m, z) v_{n,m} - (g_{12} |u_{n,m}|^2 + g_{22} |v_{n,m}|^2) v_{n,m}. \end{aligned} \quad (19)$$

Of course, these 2D fractional DNLS equations can also be extended to the 3D case.

**Remark 2** When  $C_\alpha = C_\beta = C$ ,  $\alpha = \beta$ , Eq. (14) reduces to

$$i \frac{du_{n,m}}{dz} = C \left\{ \left[ \left( -\frac{\widehat{\partial}^2}{\partial n^2} \right)^{\alpha/2} + \left( -\frac{\widehat{\partial}^2}{\partial m^2} \right)^{\alpha/2} \right] u \right\}_{n,m} - g |u_{n,m}|^2 u_{n,m}, \quad (20)$$

It follows from the definition of the discrete fractional derivative that quasi-1D model Eq. (20) with same LI is different from Eq. (13) with the single LI.

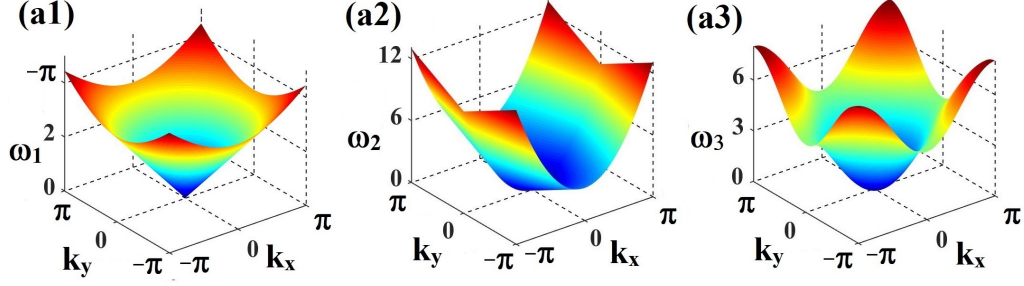


Figure 1: Different types of linear DRs: for Eq. (13) it is  $\omega_1(k)$  with LI  $\alpha = 1$  (a1), for Eq. (14) it is  $\omega_2(k)$  with LIs  $\alpha = 2, \beta = 1$  (a2), and for Eq. (28) it is  $\omega_3(k)$  (a3). The coupling coefficients are  $C = C_\alpha = C_\beta = 1$ .

**Remark 3** The following relations hold for the discrete fractional derivatives of the CW:

$$\left\{ \left( -\frac{\widehat{\partial}^2}{\widehat{\partial}n^2} - \frac{\widehat{\partial}^2}{\widehat{\partial}m^2} \right)^{\alpha/2} e^{ik \cdot \mathbf{r}} \right\}_{n,m} = |\mathbf{k}|^\alpha e^{ik \cdot \mathbf{r}}, \quad (21)$$

$$\left\{ \left( -\frac{\widehat{\partial}^2}{\widehat{\partial}n^2} \right)^{\alpha/2} e^{ik \cdot \mathbf{r}} \right\}_{n,m} = |k_x|^\alpha e^{ik \cdot \mathbf{r}},$$

with  $\mathbf{k} = (k_x, k_y)$  and  $\mathbf{r} = (n, m)$ . They can be substantiated through a straightforward Fourier expansion, and are utilized below. The proof of these relations is presented in Appendix A.

**Remark 4** In the limits of LIs  $\alpha = \beta = 1$ , which is opposite to the one corresponding to the non-fractional diffraction ( $\alpha = \beta = 2$ ), the fractional Laplacians with exponents  $\alpha/2$  or/and  $\beta/2$  in Eqs. (13) and (14) reduce to the relativistic operators widely used in mathematical physics [16, 103, 104]. In this case, Eqs. (13) and (14) become

$$i \frac{du_{n,m}}{dz} = C \left\{ \left( -\frac{\widehat{\partial}^2}{\widehat{\partial}n^2} - \frac{\widehat{\partial}^2}{\widehat{\partial}m^2} \right)^{1/2} u \right\}_{n,m} - g|u_{n,m}|^2 u_{n,m}, \quad (22)$$

and

$$i \frac{du_{n,m}}{dz} = \left\{ \left[ C_\alpha \left( -\frac{\widehat{\partial}^2}{\widehat{\partial}n^2} \right)^{1/2} + C_\beta \left( -\frac{\widehat{\partial}^2}{\widehat{\partial}m^2} \right)^{1/2} \right] u \right\}_{n,m} - g|u_{n,m}|^2 u_{n,m}. \quad (23)$$

### 3 Dispersion relations (DRs) and spectral band for linear modes

An essential attribute of discrete systems is encapsulated in its DR, delineating the connection between real frequency  $\omega(\mathbf{k})$  and wavenumber  $\mathbf{k}$  of small-amplitude lattice waves, commonly referred to as ‘‘phonons’’. Determined by the linearized system, the DR also defines the spectral band, which is the range of frequencies that permit the propagation of these linear waves [101].

To establish the DRs, we consider a solution of the linearized version of Eqs. (13) and (14) in the CW form,

$$u_{n,m} = \exp(i(\mathbf{k} \cdot \mathbf{r} - \omega_j(\mathbf{k})z)), \quad j = 1, 2, \quad (24)$$

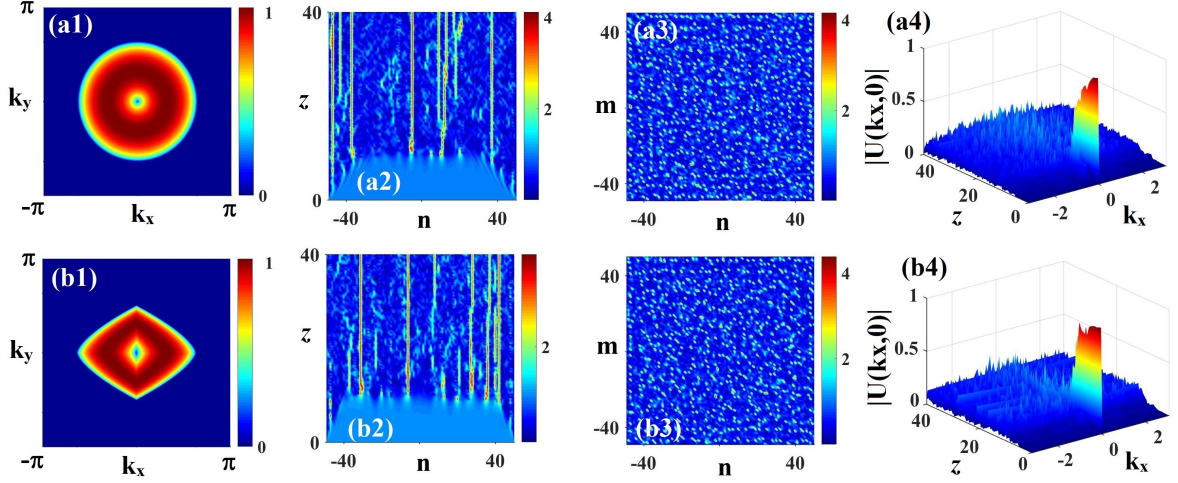


Figure 2: MI produced by Eqs. (13) (top) and (14) (bottom) with LIs  $\alpha = 1, \beta = 1.5$  and the linear-coupling coefficient  $C = 1$ . (a1,b1) The instability growth rates  $G_1$  and  $G_2$  corresponding to Eq. (37). Simulations of Eqs. (13) and (14) with input  $u_{n,m}(0) = 1 + \varepsilon_{n,m}$ : (a2,b2) The cross-section of amplitude  $|u_{n,m}(z)|$ , where  $0 \leq z \leq 40$ . S (a3,b3): The final space-time pattern at  $z = 40$ . (a4,b4): Similar to (a2,b2), but in the Fourier space.

respectively. This formulation leads to corresponding DRs in the form of

$$\omega_1(\mathbf{k}) = C \sum_{l_x=-\infty}^{+\infty} \sum_{l_y=-\infty}^{+\infty} D_{l_x, l_y}^{(\alpha)} \cos(l_x k_x + l_y k_y) \quad (25)$$

for Eq. (13) as well as

$$\omega_2(\mathbf{k}) = C \left[ \sum_{l_x=-\infty}^{+\infty} E_{l_x}^{(\alpha)} \cos(l_x k_x) + \sum_{l_y=-\infty}^{+\infty} E_{l_y}^{(\beta)} \cos(l_y k_y) \right] \quad (26)$$

for Eq. (14). A straightforward application of Fourier integrals reveals that the aforementioned expressions can be simplified to:

$$\begin{aligned} \omega_1(\mathbf{k}) &= C |\mathbf{k}|^\alpha, \\ \omega_2(\mathbf{k}) &= C (|k_x|^\alpha + |k_y|^\beta), \end{aligned} \quad (27)$$

see Appendix A for their detailed derivations.

Notably, these DRs align with that of the continuous fractional NLS equation, except for the range of the wavenumber  $\mathbf{k}$ . Furthermore, they differ from the DR of the standard 2D DNLS equation with the nearest-neighbor coupling [101, 102, 105],

$$i \frac{du_{n,m}}{dz} = C (4u_{n,m} - u_{n+1,m} - u_{n-1,m} - u_{n,m+1} - u_{n,m-1}) - g |u_{n,m}|^2 u_{n,m}, \quad (28)$$

which is

$$\omega_3(\mathbf{k}) = 2C [2 - \cos(k_x) - \cos(k_y)]. \quad (29)$$

Thus, the lattice band, defined by extremities of the DRs as specified by Eqs. (25) and (26), spans the following ranges:

$$0 \leq \omega_1(\mathbf{k}) \leq C (\sqrt{2}\pi)^\alpha, \quad 0 \leq \omega_2(\mathbf{k}) \leq C (\pi^\alpha + \pi^\beta). \quad (30)$$



Discrete solitons can emerge in the form described by Eq. (30) at frequencies outside these bands. Shown in Fig. 1 are the different types of the linear DRs for  $\omega_j(\mathbf{k})$  ( $j = 1, 2, 3$ ) with certain parameters. The DRs for Eq. (13) are displayed in Fig. 1(a1) as  $\omega_1(k)$  with LI  $\alpha = 1$ , and for Eq. (14) the DRs are displayed in Fig. 1(a2) as  $\omega_2(k)$  with LIs  $\alpha = 2$ ,  $\beta = 1$ . For Eq. (28), the DRs are displayed in Fig. 1(a3) as  $\omega_3(k)$ , with the fixed coupling coefficient  $C = 1$ . They manifest different shapes:  $\omega_1(\mathbf{k})$  features a cone, as per Eq. (27), while  $\omega_2(\mathbf{k})$  corresponds to a parabolic form in one direction and a straight line in the other one; lastly,  $\omega_3(\mathbf{k})$  exhibits a (cell of the) periodic structure.

## 4 Modulation instability (MI) and excitation of rogue waves (RWs)

Next, we address MI as the instability of CWs in the framework of the full fractional DNLS equations (13) and (14). Our initial approach considers the modulational perturbation of the spatially uniform CW,  $u_{n,m}(z) = e^{igz}$ , as

$$u_{n,m}^\epsilon(z) = (1 + \epsilon W_{n,m}(z)) e^{igz}, \quad (31)$$

with  $\epsilon \ll 1$ . Substituting Eq. (31) in Eqs. (13) and (14), and linearizing with respect to  $\epsilon$ , we derive the following equations for perturbation amplitudes  $W_{n,m}(z)$ :

$$i \frac{dW_{n,m}}{dz} = C \left\{ \left( -\frac{\widehat{\partial}^2}{\partial n^2} - \frac{\widehat{\partial}^2}{\partial m^2} \right)^{\alpha/2} W \right\}_{n,m} - g(W_{n,m} + W_{n,m}^*) = 0, \quad (32)$$

for Eq. (13) and

$$i \frac{dW_{n,m}}{dz} = C \left\{ \left[ \left( -\frac{\widehat{\partial}^2}{\partial n^2} \right)^{\alpha/2} + \left( -\frac{\widehat{\partial}^2}{\partial m^2} \right)^{\beta/2} \right] W \right\}_{n,m} - g(W_{n,m} + W_{n,m}^*) = 0, \quad (33)$$

for Eq. (14). We further assume that  $W_{n,m}$  is represented by the lowest Fourier modes as

$$W_{n,m}(z) = f_+ e^{i(\mathbf{k} \cdot \mathbf{r} - \Omega(\mathbf{k})z)} + f_- e^{-i(\mathbf{k} \cdot \mathbf{r} - \Omega(\mathbf{k})z)}. \quad (34)$$

Incorporating ansatz (34) in the linearized equations (32) and (33), we obtain a relation between the perturbation frequency and wavenumber, *viz.*,

$$\Omega^2(\mathbf{k}) = C|\mathbf{k}|^\alpha (C|\mathbf{k}|^\alpha - 2g) \quad (35)$$

for Eq. (13) and

$$\Omega^2(\mathbf{k}) = C \left( |k_x|^\alpha + |k_y|^\beta \right) \left[ C \left( |k_x|^\alpha + |k_y|^\beta \right) - 2g \right] \quad (36)$$

for Eq. (14). The derivation of these relations is given in Appendix B. Observing that the criterion for the emergence of MI is  $\Omega^2 < 0$ , we can deduce wavenumber conditions for the instability. Note that Eq. (35) is similar to the continuous 2D fractional NLS equation, differing only in the wavenumber. As a result, the range of unstable wavenumbers is the same, namely,  $|\mathbf{k}|^\alpha < 2g/C$ . The analysis naturally corroborates the absence of MI in the defocusing regime, hence we address the self-focusing case, setting  $g = 1$ . The wavenumber condition for Eq. (36) can be derived similarly. We thus identify the instability growth rates  $G_1$  and  $G_2$  (the imaginary part of  $\Omega$ ), which are associated with Eq. (35) and Eq. (36), respectively:

$$\begin{aligned} G_1 &= \sqrt{C|\mathbf{k}|^\alpha (2 - C|\mathbf{k}|^\alpha)}, \\ G_2 &= \sqrt{C \left( |k_x|^\alpha + |k_y|^\beta \right) \left[ 2 - C \left( |k_x|^\alpha + |k_y|^\beta \right) \right]}. \end{aligned} \quad (37)$$

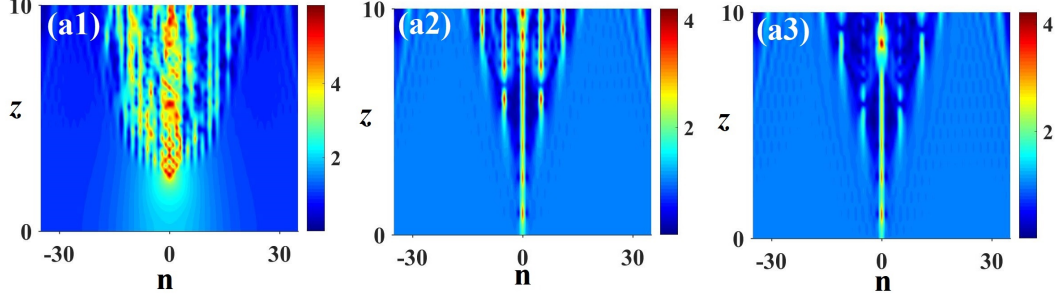


Figure 3: The RW evolution produced by simulations of Eq. (13) with parameters  $\alpha = 1.5$ ,  $C = 1$  and input given by Eq. (39), with different widths: (a1)  $w = 5$ , (a2)  $w = 0.5$ , (a3)  $w = 0.1$ . The evolution is displayed in cross section  $m = 0$ .

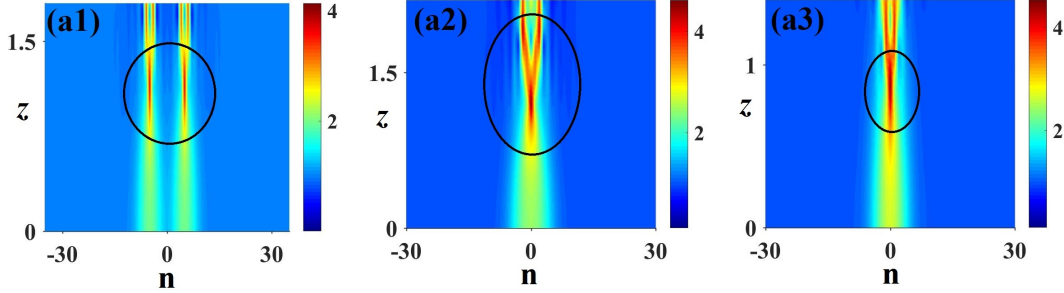


Figure 4: Different types of RWs produced by simulations of Eq. (13) with parameters  $\alpha = 1.5$ ,  $C = 1$  and input (40), with  $w = 2.5$ , for different center points: (a1)  $n_0 = 5$ , (a2)  $n_0 = 2$ , (a3)  $n_0 = 1.5$ . The evolution is displayed in cross section  $m = 0$ . The black elliptical regions delineate the high-amplitude RWs.

The expression for  $G_1$  demonstrates that the largest instability growth rate is 1, achieved on a circle of radius  $(1/C)^\alpha$  in the wavenumber space. The situation for  $G_2$  is similar, except for that the largest instability growth rate is attained at  $|k_x|^\alpha + |k_y|^\beta = 1/C$ .

A quintessential example for the MI growth rate is produced in Figs. 2(a1,b1), for  $\alpha = 1$ ,  $\beta = 1.5$ ,  $C = 1$ . To corroborate the MI prediction, we conduct numerical simulations using the initial condition

$$u_{n,m}(0) = 1 + \varepsilon_{n,m}, \quad |\varepsilon_{n,m}| \ll 1. \quad (38)$$

It is observed that small perturbations feature exponential amplification, until MI saturates due to the non-linearity of the growing perturbation. The amplification of the perturbation in the real space is accompanied by the emergence of large-amplitude structures, as seen in Figs. 2(a2,a3), where Fig. 2(a2) presents a cross-sectional view at  $m = 0$  and Fig. 2(a3) displays the spatiotemporal evolution up to  $z = 40$ . Figures 2(b2,b3) exhibit similar outcomes. Conversely, in the Fourier space, it is seen that sidebands around the original wavenumber are excited (see Figs. 2(a4,b4)), resulting in the generation of harmonics. Note that the amplitude is normalized in this analysis. A more detailed examination of the relationship between MI and LI will be reported elsewhere.

To rigorously explore RW solutions on the fractional lattice, we perform numerical investigation of Eqs. (13) and (14). To this end, we employ a Gaussian input, which is known as an effective method for triggering RW phenomena through the gradient-catastrophe mechanism in the focusing NLSE, as initially shown in the framework of the semiclassical approximation for the continuum NLS equation [106], and further corroborated by experimental findings in nonlinear optics [107].

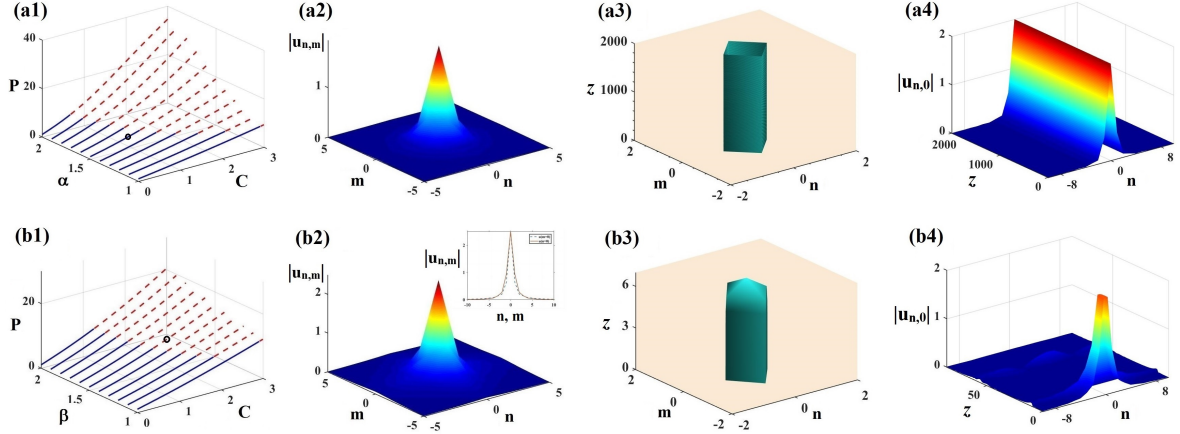


Figure 5: Fundamental solitons produced by the isotropic equation (42) (top) and anisotropic one (43) (bottom), respectively. (a1) Power  $P$  vs. the coupling constant  $C$  and LI  $\alpha$ , as produced by the numerical solutions of Eq. (42), with solid and dashed lines denoting stable and unstable segments, respectively. (a2,a3): The profile and stable evolution of the soliton with  $C = 1$  and  $\alpha = 1.5$ . (a4): The evolution in cross-section  $m = 0$ . (b1) Power  $P$  vs. the coupling constant  $C$  and LI  $\beta$ , as produced by the numerical solutions of Eq. (43) with fixed LI,  $\alpha = 1$ . (b2,b3): The profile and unstable evolution of the soliton with  $C = 2$  and  $\beta = 1.5$ . (b4): The evolution in cross-section  $m = 0$ . The inset in (b2) displays the cross-section corresponding to  $v(n, 0)$  and  $v(0, m)$ .

As an example, we do it for Eq. (13) with two different inputs (the results for Eq. (14) are quite similar):

- First, we consider Eq. (13) with fixed parameters  $\alpha = 1.5, C = 1$ , and the following initial condition:

$$u_{n,m}(0) = 1 + \exp\left(-\frac{n^2 + m^2}{2w^2}\right), \quad (39)$$

where  $w$  is the width of the input. The constant term 1 represents the normalized amplitude of the background CW, as the reference value. The choice of this input, built as the Gaussian perturbation added to the CW background, facilitates the evolution towards RWs. The variation of the wave field for different values of  $w$  are illustrated in Fig. 3, where the panels from left to right correspond to  $w = 5, w = 0.5$ , and  $w = 0.1$ , respectively. These findings reaffirm the generality of the gradient catastrophe scenario presented in Ref. [106]. Although the nonintegrability of the lattice model distorts the resulting Peregrine-soliton patterns, deviating from the “Christmas tree” structures produced in the paradigmatic NLS equation, this pattern remains recognizable. As  $w$  decreases, the RW pattern gradually evolves towards a breathing-type solution. This observation is consistent with the analysis for the integrable NLS equation outlined in Ref. [106], which has been similarly validated in various continuous [108] and discrete [109] systems. Similar results are produced by the anisotropic model based on Eq. (14) (not shown here).

- Second, it is worthy to note is that we can generate higher-order RWs from a superposition of multiple Gaussians. To this end, we numerically solve Eq. (13) with parameters  $\alpha = 1.5, C = 1$ , using the following input including two Gaussians with width  $w$  and centers placed at points  $n = \pm n_0$  (including the input with virtual centers if  $n_0$  is not integer):

$$u_{n,m}(0) = 1 + \exp\left(-\frac{(n - n_0)^2}{2w^2}\right) + \exp\left(-\frac{(n + n_0)^2}{2w^2}\right). \quad (40)$$

Here, we consider motion along the  $n$ -direction, although movement in the  $(n, m)$  direction could also be explored. Different forms of RWs generated by this input with  $w = 2.5$  are displayed in Fig. 4. Initially, for  $n_0 = 5$ , a symmetric RW is obtained in Fig. 4(a1). As  $n_0$  is reduced to 2, a tri-RW state emerges, where the wave initially concentrates into a single RW before splitting into two separate ones in Fig. 4(a2). Further decreasing  $n_0$  to 1.5 reveals a significantly stronger tri-RW, as shown in Fig. 4(a3).

## 5 2D nonlinear modes and their stability

In this section, we conduct a comprehensive investigation of fundamental and vortical solitons produced by the isotropic and anisotropic models based on Eqs. (13) and (14). The analysis encompasses their existence conditions and stability properties.

Localized stationary modes are looked for in the usual form,

$$u_{n,m}(z) = v_{n,m}e^{-i\omega z}, \quad v_{n,m} = v(n, m) \quad (41)$$

for the 2D fractional DNLS equations (13) and (14) with  $g = 1$  (the normalized self-focusing nonlinearity) and real frequency  $\omega$ . Substituting this in Eqs. (13) and (14) leads to the stationary equations,

$$C \left( -\frac{\widehat{\partial}^2}{\widehat{\partial}n^2} - \frac{\widehat{\partial}^2}{\widehat{\partial}m^2} \right)^{\alpha/2} v_{n,m} - |v_{n,m}|^2 v_{n,m} = \omega v_{n,m}, \quad (42)$$

and

$$C \left[ \left( -\frac{\widehat{\partial}^2}{\widehat{\partial}n^2} \right)^{\alpha/2} + \left( -\frac{\widehat{\partial}^2}{\widehat{\partial}m^2} \right)^{\beta/2} \right] v_{n,m} - |v_{n,m}|^2 v_{n,m} = \omega v_{n,m}. \quad (43)$$

In these equations,  $\omega$  can be scaled out by defining  $v_{n,m} \equiv \sqrt{-\omega} \widehat{v}_{n,m}$  and  $C \equiv -\omega \widehat{C}$ . Henceforth, we fix  $\omega = -1$  ( $\omega < 0$  is necessary for the creation of bright-soliton solutions).

The 2D nonlinear fractional-difference equation (42) can be solved numerically, starting from the anti-continuum (ac) limit,  $C = 0$  [105, 110]. In this limit, the solution of Eq. (42) is obvious:

$$v_{n,m}^{(0)} = \begin{cases} e^{i\theta_{n,m}}, & (n, m) \in S, \\ 0, & (n, m) \in \mathbb{Z}^2 \setminus S, \end{cases} \quad (44)$$

where  $S$  is a finite set of nodes on the square lattice  $(n, m) \in \mathbb{Z}^2$  and  $\theta_{n,m}$  are phases of the populated (nonzero) sites. In particular, discrete solitons and vortices correspond to  $\theta_{n,m} = 0$  and  $\theta_{n,m} \in [0, 2\pi]$ , respectively. The existence of the continuous family of solitons branching from Eq. (44) at finite values of  $C$  can be rigorously proven using the implicit function theorem [105, 110].

The linear stability analysis of the standing-wave solutions can be performed in the framework of the linearized Bogoliubov-de Gennes equations for small perturbations. Substituting the perturbed solution

$$u_{n,m}(z) = \left[ v_{n,m} + \epsilon \left( a_{n,m} e^{\lambda z} + b_{n,m}^* e^{\lambda^* z} \right) \right] e^{-i\omega z} \quad (45)$$

with  $\epsilon \ll 1$  in Eq. (13), one derives the eigenvalue problem for the perturbation amplitudes  $(a_{n,m}, b_{n,m})$  and instability growth rate  $\lambda$ ,

$$\begin{pmatrix} L_{11} & L_{12} \\ -L_{12}^* & -L_{11}^* \end{pmatrix} \begin{pmatrix} a_{n,m} \\ b_{n,m} \end{pmatrix} = i\lambda \begin{pmatrix} a_{n,m} \\ b_{n,m} \end{pmatrix}, \quad (46)$$

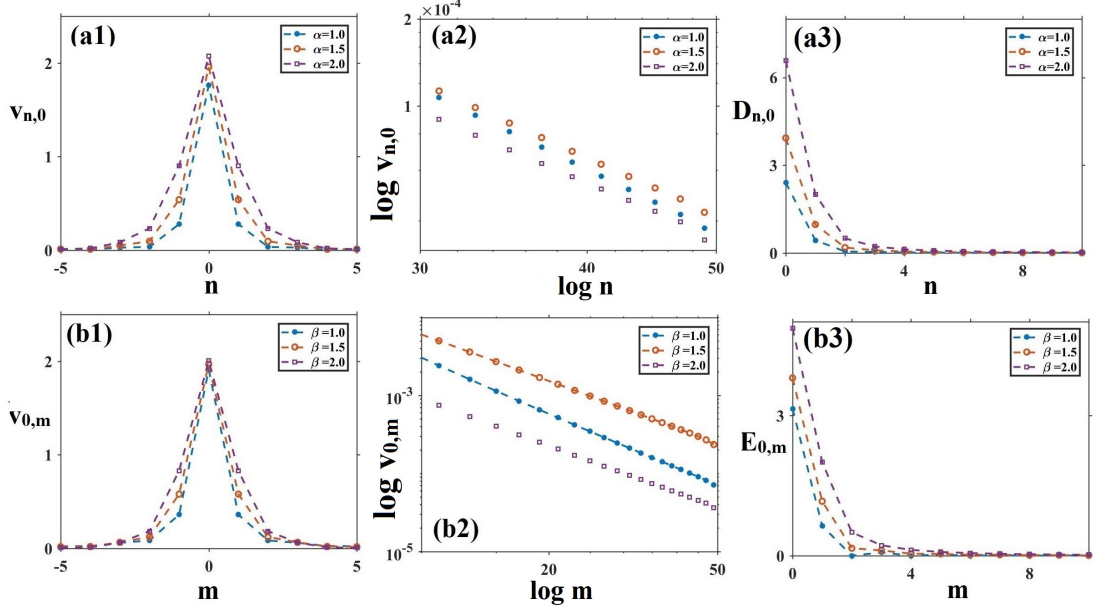


Figure 6: Solitons produced by Eq. (42) with fixed  $C = 1$ , and different typical values of LI:  $\alpha = 1, 1.5, 2.0$ : (a1) Cross-section  $v_{n,0}$ ; (a2) tails of the soliton profiles from panel (a1) on the log-log scale; (a3) the effective coupling constant between lattice sites  $(0, 0)$  and  $(n, 0)$ . According to the data displayed in panel (a2), the decaying tail may be approximated by  $v_{n,0} \sim |n|^{-\eta}$  with  $\eta = 1.80, 1.77, 1.67$  corresponding to  $\alpha = 1, 1.5, 2.0$ , respectively. Solitons produced by (anisotropic) Eq. (43) with fixed  $\alpha = 1, C = 1$ , and typical values of the second LI:  $\beta = 1, 1.5, 2.0$ : (b1) a typical cross-section  $v_{0,m}$ ; (b2) tails of the soliton profiles from panel (b1) on the log-log scale, the respective decay powers being  $\eta = 2.38, 2.16, 1.99$  for  $\beta = 1, 1.5, 2.0$ , respectively; (b3) the effective coupling constant between lattices site  $(0, 0)$  and  $(0, m)$ .

where

$$\begin{aligned}
 L_{11} &= C \left( -\frac{\widehat{\partial}^2}{\widehat{\partial} n^2} - \frac{\widehat{\partial}^2}{\widehat{\partial} m^2} \right)^{\alpha/2} - 2|v_{n,m}|^2 - \omega, \\
 L_{12} &= -v_{n,m}^2.
 \end{aligned} \tag{47}$$

Similarly, we deduce the corresponding eigenvalue problem for Eq. (14), with the different operator

$$L_{11} = C \left[ \left( -\frac{\widehat{\partial}^2}{\widehat{\partial} n^2} \right)^{\alpha/2} - \left( \frac{\widehat{\partial}^2}{\widehat{\partial} m^2} \right)^{\beta/2} \right] - 2|v_{n,m}|^2 - \omega. \tag{48}$$

The discrete soliton  $u_{n,m}(z)$  is unstable if there exists at least a single eigenvalue with  $\text{Re}(\lambda) > 0$ . Predictions of the linear-stability analysis are then verified by direct simulations of the perturbed evolution, running them by dint of the fourth-order Runge-Kutta method [111]. In the course of the simulations, the conservation of Hamiltonian (15) and power (17) was monitored to control the accuracy of the numerical scheme.

## 5.1 Fundamental (zero-vorticity) solitons and their stability

We begin the analysis with the existence and stability of fundamental solitons produced by Eqs. (42) and (43), starting from the anti-continuum (AC) limit,  $C = 0$  [101, 112].

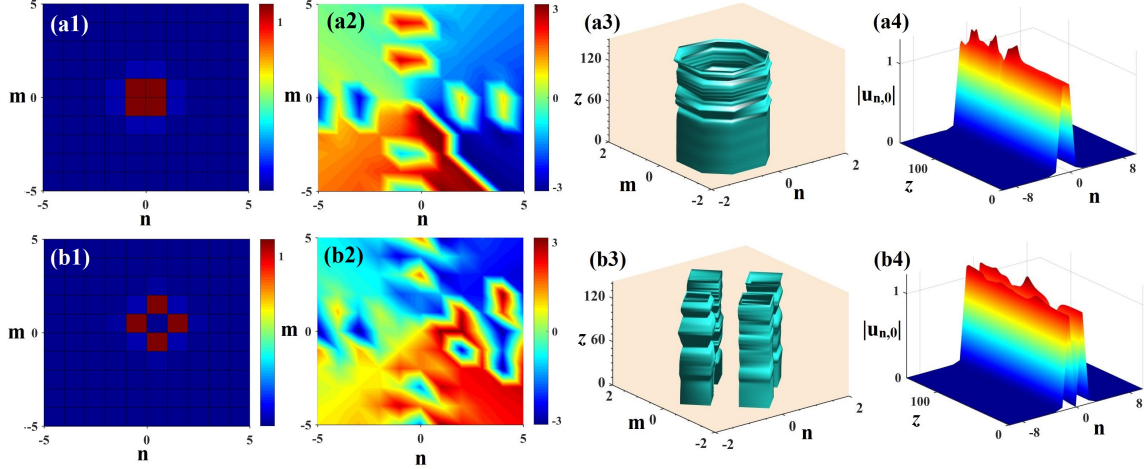


Figure 7: A typical unstable vortex soliton produced by Eq. (42) with LI  $\alpha = 1$  and  $C = 0.1$ . (a1,a2) The intensity and phase patterns of an intersite-centered soliton. The unstable evolution is displayed in panels (a3) and (a4). The second row is similar to the first one, representing a typical unstable onsite-centered vortex soliton.

*Case 1: The isotropic model.*—Results for fundamental isotropic solitons produced by Eq. (42) are summarized in Fig. 5(a1) in the form of dependences of the total power  $P$  (see Eq. (17)) on LI,  $\alpha \in (1, 2]$ , and coupling constant  $C \in [0, 3]$ . As mentioned above, in the continuous 2D fractional NLS equation, solitons (including ones of the fundamental and vortex types) are destabilized by the critical and supercritical collapse at  $\alpha = 2$  and  $\alpha < 2$ , respectively. However, the destabilization is forestalled in the discrete setting, as shown in Fig. 5(a1), where the stability area is indicated by solid curves. It is seen that the stability domain of the fundamental solitons increases with the decrease of LI  $\alpha$ , which is explained by the weaker interactions between sites of the discrete medium. To illustrate this feature in detail, we display the effective coupling constant  $D_{l_x, l_y}^{(\alpha)}$  between sites  $(0, 0)$  and  $(n, 0)$  with fixed  $C = 1$ , for typical values of LI,  $\alpha = 1, 1.5, 2.0$ , in Fig. 6(a3). It is seen that coefficient  $D_{l_x, l_y}^{(\alpha)}$  indeed decreases with the decrease of LI  $\alpha$ . Another conclusion suggested by Fig. 5(a1) is that the  $P(C)$  curves shift down as  $\alpha$  decreases.

It is known that fractional solitons produced by the continuous fractional NLS equations display a power-law decay of their tails [38, 113, 114]. As an illustrative example, one can take the 1D linear fractional equation (3) with  $V(x) = 0$  and substitute a trial Lorentzian profile

$$u_{\text{Lorentz}}(x) = \left(x^2 + x_0^2\right)^{-1} e^{-i\mu t} \quad (49)$$

in the fractional-diffraction term. Then, a straightforward calculation of that term yields the following asymptotic result, at  $x^2 \rightarrow \infty$ :

$$\left(-\frac{\partial^2}{\partial x^2}\right)^{\alpha/2} u_{\text{Lorentz}}(x) \Big|_{\text{at } x^2 \gg x_0^2} \approx -\frac{\Gamma(\alpha + 1)}{8x_0} |x|^{-(\alpha+1)} e^{-i\mu t} \quad (50)$$

(here  $x_0 > 0$  is adopted by definition). Taking into regard the first term in Fig. (3), one concludes that Eq. (3) with  $\alpha = 1$  yields a self-consistent power-law tail  $\sim |x|^{-2}$ , the respective chemical potential being  $\mu = -(8x_0)^{-1}$ . Note that the numerically found decay rate of the tail in the 2D discrete system with  $\alpha = 1$ ,  $\eta = 1.80$  (see the caption to Fig. 6), is indeed close to value  $\eta = 2$  produced by the present analysis for the 1D continuous fractional system.

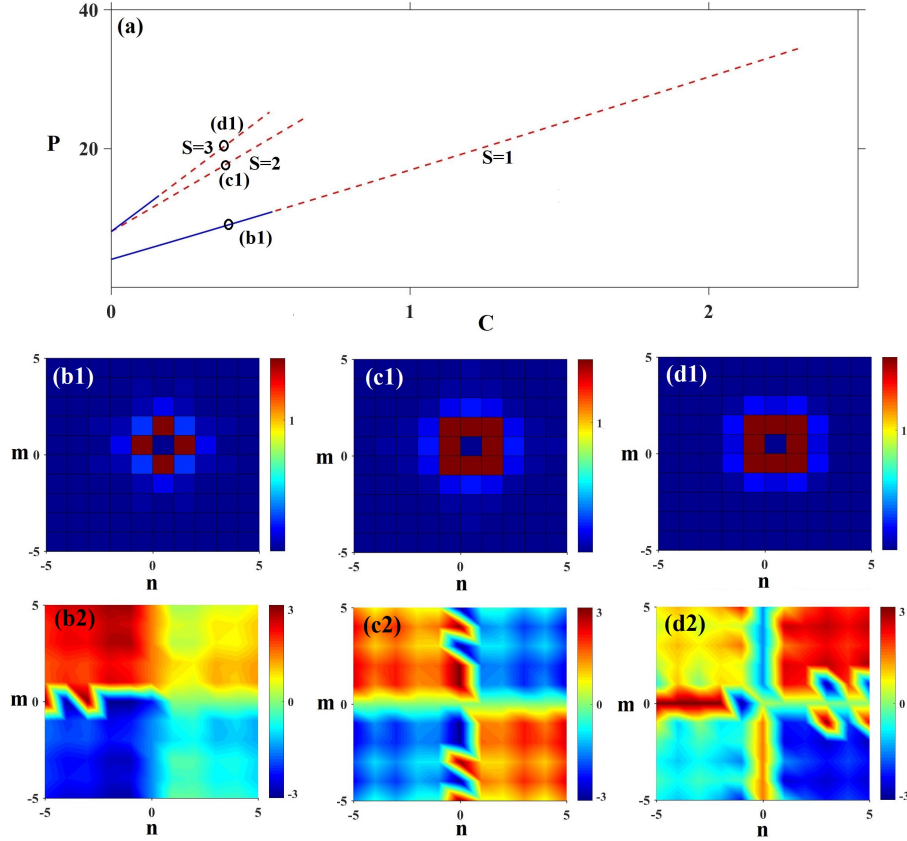


Figure 8: Quasi-isotropic vortex solitons produced by the symmetric equation (43) with LIs  $\alpha = \beta = 1$ . (a) Power  $P$  vs.  $C$  with different vorticities  $S = 1, 2, 3$ , where solid and dashed lines denote stable and unstable families of the vortex solitons, respectively. (b1,b2) The intensity and phase structures of the discrete vortex soliton with  $S = 1$  at  $C = 0.4$ . (c1,c2) The same as in (b1,b2) but for  $S = 2$ . (d1,d2) The same as in (b1,b2), but for  $S = 3$ .

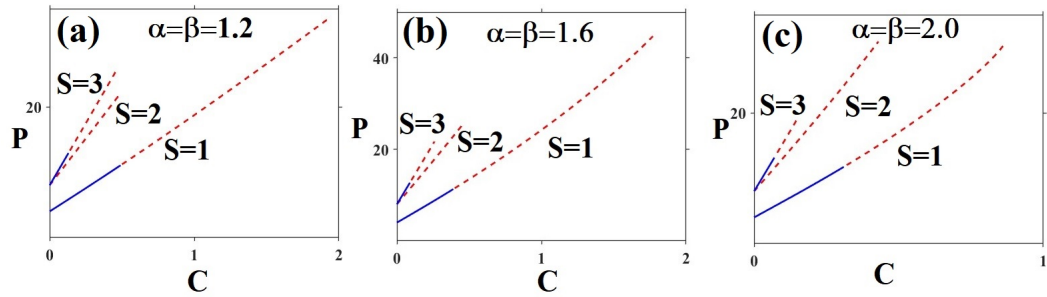


Figure 9: Quasi-isotropic vortex solitons produced by the symmetric equation (43) with different LIs at (a)  $\alpha = \beta = 1.2$ , (b)  $\alpha = \beta = 1.6$  as well as at (c)  $\alpha = \beta = 2.0$ . The blue solid line and the red dashed line represent stable and unstable vortex solitons, respectively.

For the present discrete fractional model, representative shapes of the solitons with fixed  $C = 1$  are potted in Fig. 6(a1), Their tails are displayed in Fig. 6(a2) on the log-log scale. The results demonstrate a power-law decay of their tails, with the decay rates (their values are given in the caption to Fig. 6) increasing with the decrease of LI  $\alpha$ , which is again explained by the weaker coupling between sites of the



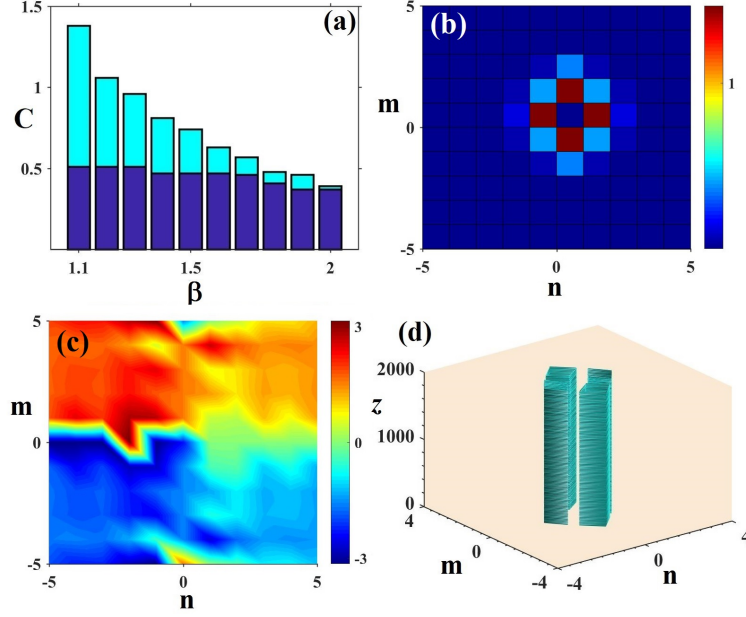


Figure 10: Anisotropic vortex solitons produced by the 2D asymmetric fractional DNLS equation (43) with  $\alpha \neq \beta$ . (a) The existence and stability regions of the discrete vortex solitons with  $S = 1$ , for different values of LI  $\beta$  and fixed  $\alpha = 1$ . Green and blue bars represent the existence and stability regions, respectively. (b,c) The intensity and phase structure of the stable discrete vortex soliton with  $S = 1$ ,  $C = 0.3$  as well as  $\beta = 2$ . (d) The stable perturbed evolution of the same vortex soliton.

lattice, corresponding to smaller values of coefficients  $D_{l_x, l_y}^{(\alpha)}$  (see Fig. 6(a3)). A typical profile of a stable 2D fundamental soliton with  $\alpha = 1.5$  and  $C = 1$  is displayed in Fig. 5(a2). Its stability is corroborated by simulating its perturbed evolution, which is displayed in Figs. 5(a3,a4).

*Case 2: The anisotropic model.*—To demonstrate results for fundamental solitons produced by the anisotropic model based on Eq. (43), we focus on the characteristic case with fixed LI  $\alpha = 1$  and varying the other LI,  $\beta \in (1, 2]$ . The dependence of power  $P$  on  $\beta$  and coupling constant  $C$  is presented in Fig. 5(b1). Similar to the case of the isotropic model (cf. Fig. 5(a1)), the stability region increases as  $\beta$  decreases, as a consequence of the change of effective coupling constant  $E_{l_x, l_y}^{(\alpha)}$  with fixed  $C = 1$ , as shown in Fig. 6(b3). The cross-section profiles of the fundamental solitons are displayed in Fig. 6(b1) for different values of the second LI  $\beta$ , and their tails are shown, on the log-log scale, in Fig. 6(b2), verifying the power-law decay of the tails.

A typical example of an unstable fundamental soliton in the anisotropic model, with LIs  $\alpha = 1$ ,  $\beta = 1.5$  and coupling constant  $C = 2$ , is displayed in Fig. 5(b2). Its unstable evolution is shown in Figs. 5(b3,b4), with the intensity decaying to zero.

## 5.2 Vortex solitons and their stability

The consideration of vortex solitons with integer winding numbers  $S = 1, 2, 3, \dots$ , is another natural subject in the study of the 2D fractional DNLS models.

First, extensive simulations of the isotropic equation (42) demonstrate that this model readily supports stationary vortex solitons, but they are all unstable. Typical examples of unstable intersite- and onsite-centered vortex solitons with  $S = 1$  are displayed in Fig. 7 for  $\alpha = 1$  and  $C = 0.1$ . As usual, the phase sin-



gularity of a vortex occurs at the point where the amplitude of the solution is vanishing. Simulations of the perturbed evolution of these solitons, displayed in Figs. 7(a3,a4) and (b3,b4), demonstrate their spontaneous transformation into breathers that perform apparently randomized oscillations. This is different from the usual behavior of unstable vortex solitons, which demonstrate splitting into separating fragments [105,115].

Next, the stability of quasi-isotropic vortex solitons of the symmetric equation (43) with equal LIs,  $\alpha = \beta = 1$ , and different vorticities  $S = 1, 2, 3$  are summarized in Fig. 8(a). Naturally, the region for the coupling constant  $C$  supporting the existence of the vortex solitons shrinks with the increase of  $S$ . The curves in Fig. 8(a) abort when they hit the boundary of the existence area of the vortex solitons. We find *stable* quasi-isotropic vortex solitons with winding numbers  $S = 1$  and 3, while ones with  $S = 2$  are completely unstable, similar to what has been reported in previously studied non-fractional lattice models with the nearest-neighbor coupling [105,115]. Some representative examples of the local-power and phase structure of the vortex solitons are shown for  $C = 0.4$  in Figs. 8(b1,b2,c1,c2,d1,d2). The comparison with previous (non-fractional) models [110,115] suggests that the present fractional one, based on Eq. (43), gives rise to a broader stability area for the vortex solitons. Additionally, we have considered quasi-isotropic vortex solitons in the model with different LIs, and the topological charge ranging from 1 to 3, see the results in Fig. 9. One observes in the figure that both the existence and stability ranges of the solitons decrease as  $\alpha$  increases, similar to the above-mentioned results for the fundamental solitons, primarily due to the change in the effective coupling coefficient.

Finally, we consider the asymmetric vortex solitons produced by the anisotropic equation (43), with different LIs  $\alpha \neq \beta$ . Results are summarized in Fig. 10(a) for different values of LI  $\beta$ , fixing  $\alpha = 1$ . Only discrete vortex solitons with  $S = 1$  are found in this model. Their existence and stability regions, represented by green and blue bars, respectively, in Fig. 10(a), shrink as  $\beta$  decreases. A typical stable onsite-centered vortex soliton with  $S = 1$  is presented for  $C = 0.3$  in Figs. 10(b,c), where the soliton's anisotropy is clearly seen. The stable perturbed evolution of the same vortex soliton is demonstrated in Fig. 10(d) by means of isosurfaces.

## 6 Conclusions and discussions

In the present work, we have proposed the novel models of 2D fractional dynamical lattices, based on fractional DNLS equations. The new discrete versions of the quasi-RFD (Riesz fractional derivative) and Laplacian, characterized by the respective LIs (Lévy indices), are naturally introduced by means of the respective direct and inverse Fourier transform. One 2D fractional DNLS equation includes the isotropic fractional Laplacian with LI  $\alpha \in (1, 2]$ . The anisotropic model makes use of the fractional DNLS equation with the discrete derivatives acting independently on two spatial coordinates in the 2D lattice, each one characterized by its own LI,  $\alpha$  and  $\beta$ , and respective lattice coupling constants,  $C_\alpha$  and  $C_\beta$ . The symmetric version of the latter model, with  $\alpha = \beta$  and  $C_\alpha = C_\beta$ , is considered too. The non-fractional version of the models, with LI = 2, introduces the novel lattice system, which includes the long-range couplings  $\sim (-1)^l l^{-2}$  in the two directions between lattice sites separated by integer distance  $l$ . Utilizing this definition, the exact linear DRs (dispersion relations) and MI (modulational instability) of CWs (continuous waves, alias plane waves) are rigorously derived, exhibiting congruence with their continuous analogs. The generation of RWs (rogue waves) has been investigated by means of simulations of the underlying equations with Gaussian inputs.

Unlike the continuum fractional NLS equations in the 2D space, the underlying lattice structure arrests the onset of the collapse, thus making it possible to predict stable fundamental and vortical solitons. The formation and stability of the soliton families are explored in detail, starting from the ac (anti-continuum)

limit. The stability is established by means of the linear-stability analysis and verified by direct simulations. On the contrary to the situation in the continuum limit, when smaller LI makes the setting more prone to the onset of the collapse and resulting destabilization of solitons, in the discrete systems smaller LI values favor the stability of the solitons, which is explained by weaker coupling between the lattice sites. The isotropic model supports stable fundamental solitons, while all the vortical modes are unstable. On the other hand, the symmetric system with independent fractional derivatives acting along the two discrete coordinates maintains stable vortex-soliton families with winding numbers  $S = 1$  and  $3$ . Furthermore, the anisotropic system with  $\alpha \neq \beta$  produces stable vortex solitons with  $S = 1$ .

As an extension of the analysis, it may be interesting to consider the 2D discrete system on more sophisticated underlying lattices, such as triangular, hexagonal, and quasiperiodic ones. Similarly, it may be relevant to consider the 1D discrete system based on a quasiperiodic 1D lattice.

Another relevant direction may be the investigation of 2D fractional media with the semi-discrete structure [116], i.e., the continuum fractional derivative acting along one coordinate, and the discrete fractional derivative acting in the perpendicular direction, the respective LIs being different too. For example, the 2D fractional semi-discrete NLS equation is

$$i \frac{du_m}{dz} = \left[ C_\alpha \left( -\frac{\partial^2}{\partial x^2} \right)^{\alpha/2} + C_\beta \left( -\frac{\widehat{\partial}^2}{\widehat{\partial} m^2} \right)^{\beta/2} \right] u_m + V(x, m)u_m + F(x, m, |u_m|^2)u_m, \quad (51)$$

where  $u_m = u(x, m, z)$  is an envelope field of continuous variables  $x, z \in \mathbb{R}$  and discrete one  $m \in \mathbb{Z}$ , the LIs  $\alpha, \beta \in (1, 2]$ ,  $F(\cdot)$  is a function of  $x, m, |u_m|^2$ , and  $V(x, m)$  is a real or complex ( $\mathcal{PT}$ -symmetric) external potential.

A challenging possibility is to implement the fractional discrete setting in the 3D geometry – for example, in the form of the 3D isotropic fractional DNLS equation,

$$i \frac{du_{n,m,s}}{dz} = C \left\{ \left( -\frac{\widehat{\partial}^2}{\widehat{\partial} n^2} - \frac{\widehat{\partial}^2}{\widehat{\partial} m^2} - \frac{\widehat{\partial}^2}{\widehat{\partial} s^2} \right)^{\alpha/2} u \right\}_{n,m,s} + V(m, n, s)u_{n,m,s} + F(n, m, s, |u_{n,m,s}|^2)u_{n,m,s}, \quad (52)$$

and the 3D anisotropic fractional DNLS equation,

$$i \frac{du_{n,m,s}}{dz} = \left\{ \left[ C_\alpha \left( -\frac{\widehat{\partial}^2}{\widehat{\partial} n^2} \right)^{\alpha/2} + C_\beta \left( -\frac{\widehat{\partial}^2}{\widehat{\partial} m^2} \right)^{\beta/2} + C_\gamma \left( -\frac{\widehat{\partial}^2}{\widehat{\partial} s^2} \right)^{\gamma/2} \right] u \right\}_{n,m,s} + V(m, n, s)u_{n,m,s} + F(n, m, s, |u_{n,m,s}|^2)u_{n,m,s}, \quad (53)$$

where  $u_{n,m,s} = u(n, m, s, z)$  is an envelope field of continuous variable  $z \in \mathbb{R}$  and discrete ones  $n, m, s \in \mathbb{Z}$ , the LIs are  $\alpha, \beta, \gamma \in (1, 2]$ ,  $F(\cdot)$  is a function of  $n, m, s, |u_{n,m,s}|^2$ , and  $V(n, m, s)$  is a real or complex external potential.

## ACKNOWLEDGMENTS

The work of Z.Y. was supported by the National Natural Science Foundation of China (Nos. 11925108 and 12471242). The work of B.A.M. is supported, in part, by grant No. 1695/22 from the Israel Science Foundation.

## CONFLICT OF INTEREST STATEMENT

We declare we have no competing interests.

#### DATA AVAILABILITY STATEMENT

The data that support the findings of this study are available on a reasonable request from the corresponding author.

#### Appendix A. Derivations of Remark 3 and Eq. (27) from the main text:

For the first equality in Eq. (21), we note that the coupling coefficient  $D_{l_x, l_y}^{(\alpha)}$  in Eq. (9) can be written as

$$D_{l_x, l_y}^{(\alpha)} = \frac{1}{4\pi^2} \int_{-\pi}^{+\pi} \int_{-\pi}^{+\pi} e^{i(k_x l_x + k_y l_y)} (k_x^2 + k_y^2)^{\alpha/2} dk_x dk_y, \quad (\text{A.1})$$

due to the evenness/oddness of the trigonometric functions. Considering the definition of the fractional derivatives in Eq. (8), one can obtain

$$\begin{aligned} \left\{ \left( -\frac{\widehat{\partial}^2}{\widehat{\partial} n^2} - \frac{\widehat{\partial}^2}{\widehat{\partial} m^2} \right)^{\alpha/2} e^{i\mathbf{k}\cdot\mathbf{r}} \right\}_{n,m} &= \sum_{l_x, l_y = -\infty}^{+\infty} D_{l_x, l_y}^{(\alpha)} e^{i(k_x(n+l_x) + k_y(m+l_y))} \\ &= \sum_{l_x, l_y = -\infty}^{+\infty} D_{l_x, l_y}^{(\alpha)} e^{i(k_x l_x + k_y l_y)} e^{i\mathbf{k}\cdot\mathbf{r}} \\ &= (k_x^2 + k_y^2)^{\alpha/2} e^{i\mathbf{k}\cdot\mathbf{r}}, \end{aligned} \quad (\text{A.2})$$

where the last equality comes from the symmetry of  $(k_x^2 + k_y^2)^{\alpha/2}$  ( $= |\mathbf{k}|^\alpha$ ) and periodicity. Similarly, the second equality in Eq. (21) can be also derived.

Eqs. (25) and (26) respectively yield the first and second expressions in Eq. (27), closely aligning with the derivation of Remark 3 mentioned above. For example, the second equality in Eq. (27) is derived from Eq. (26) by noting the expression for  $E_{l_x}^{(\alpha)}$  in Eq. (11), i.e.,

$$E_{l_x}^{(\alpha)} = \frac{1}{\pi} \int_0^\pi \cos(k_x l_x) k_x^\alpha dk_x, \quad (\text{A.3})$$

as well as the expression for  $E_{l_y}^{(\beta)}$ ,

$$E_{l_y}^{(\beta)} = \frac{1}{\pi} \int_0^\pi \cos(k_y l_y) k_y^\beta dk_y. \quad (\text{A.4})$$

Substituting them into Eq. (26), and considering the symmetry and periodicity of  $|k_x|^\alpha$  and  $|k_y|^\beta$  over the interval  $[-\pi, \pi]$ , we obtain

$$\omega_2(\mathbf{k}) = C(|k_x|^\alpha + |k_y|^\beta). \quad (\text{A.5})$$

In fact,  $E_{l_x}^{(\alpha)}$  and  $E_{l_y}^{(\beta)}$  are the Fourier expansion coefficients of  $|k_x|^\alpha$  and  $|k_y|^\beta$  over the interval  $[-\pi, \pi]$ , respectively. The first equality in Eq. (27) can be derived from Eq. (25) similarly.

#### Appendix B. Derivations of Eqs. (35) and (36):

Here we show how to derive Eq. (35), the derivation of Eq. (36) being similar. Substituting Eq. (34) into Eq. (32) and considering coefficients of  $e^{i(\mathbf{k}\cdot\mathbf{r} - \Omega(\mathbf{k})z)}$  and  $e^{-i(\mathbf{k}\cdot\mathbf{r} - \Omega(\mathbf{k})z)}$  separately, we obtain

$$\begin{aligned} \Omega f_1 - C|\mathbf{k}|^\alpha f_1 + g f_1 + g f_2 &= 0, \\ \Omega f_2 + C|\mathbf{k}|^\alpha f_2 - g f_2 - g f_1 &= 0. \end{aligned} \quad (\text{B.1})$$

The derivation here also relies on the equation in Remark 3, for which we provided a proof in the above text. The necessary and sufficient condition for the above-mentioned homogeneous linear system to have a solution in terms of  $(f_1, f_2)$  is that the vanishing of the determinant of the coefficient matrix. Thus we derive

$$\Omega^2 = (C|\mathbf{k}|^\alpha - 1)^2 - 1, \quad (\text{B.2})$$

which is precisely Eq. (35).

## References

- [1] Hilfer R. *Applications of Fractional Calculus in Physics*. World Scientific; 2000.
- [2] Sabatier J, Agrawal OP, Machado JAT. *Advances in Fractional Calculus: Theoretical Developments and Applications in Physics and Engineering*. Springer; 2007.
- [3] Tarasov VE. *Fractional Dynamics: Applications of Fractional Calculus to Dynamics of Particles, Fields and Media*. Springer; 2011.
- [4] Shlesinger MF, Zaslavsky GM, Klafter J. Strange kinetics. *Nature*. 1993;363:31.
- [5] Samorodnitsky G, Taqqu MS. *Stable Non-Gaussian Random Processes*. Chapman and Hall; 1994.
- [6] Metzler R, Klafter J. The random walk's guide to anomalous diffusion: a fractional dynamics approach. *Phys Rep*. 2000;339:1-77.
- [7] Zaslavsky GM. Chaos, fractional kinetics, and anomalous transport. *Phys Rep*. 2002;371:461.
- [8] Laskin N. Fractional quantum mechanics and Lévy path integrals. *Phys Lett A*. 2000;268:298-305.
- [9] Laskin N. Fractional Schrödinger equation. *Phys Rev E*. 2002;66:056108.
- [10] Guo X, Xu M. Some physical applications of fractional Schrödinger equation. *J Math Phys*. 2006;47:082104.
- [11] Petroni NC, Pusterla M. Lévy processes and Schrödinger equation. *Physica A*. 2009;388:824.
- [12] Stickler BA. Potential condensed-matter realization of space-fractional quantum mechanics: the one-dimensional Lévy crystal. *Phys Rev E*. 2013;88:012120.
- [13] Laskin N. *Fractional Quantum Mechanics*. World Scientific; 2018.
- [14] Barthelemy P, Bertolotti J, Wiersma DS. A Lévy flight for light. *Nature*. 2008;453:495-8.
- [15] Mercadier N, Guerin W, Chevrollier M, Kaiser R. Lévy flights of photons in hot atomic vapours. *Nat Phys*. 2009;5:602-605.
- [16] Longhi S. Fractional Schrödinger equation in optics. *Opt Lett*. 2015;40:1117-1120.
- [17] Liu S, Zhang Y, Malomed BA, Karimi E. Experimental realizations of the fractional Schrödinger equation in the temporal domain. *Nat Comm*. 2023;14:222.
- [18] Zhang Y, Liu X, Belić MR, Zhong W, Zhang Y, Xiao M. Propagation dynamics of a light beam in a fractional Schrödinger equation. *Phys Rev Lett*. 2015;115:180403.
- [19] Zhang Y, Zhong H, Belić MR, Zhu Y, Zhong W, Zhang Y, Christodoulides DN, Xiao M.  $\mathcal{PT}$ -symmetry in a fractional Schrödinger equation. *Laser Photonics Rev*. 2016;10:526-531.
- [20] Liu S, Zhang Y, Malomed BA, Karimi E. Experimental realizations of the fractional Schrödinger equation in the temporal domain. *Nat Comm*. 2023;14:222.
- [21] Monje CA, Chen YQ, Vinagre BM, Xue D, Feliu V. *Fractional-order systems and controls*. Springer; 2010.
- [22] Stephanovich VA, Kirichenko EV, Engel G, Sinner A. Spin-orbit-coupled fractional oscillators and trapped Bose-Einstein condensates. *Phys Rev E*. 2024;109:014222.

- [23] Uchaikin V, Sibatov R. *Fractional kinetics in solids: Anomalous charge transport in semiconductors, dielectrics and nanosystems*. World Scientific; 2013.
- [24] Oldham KB, Spanier J. *The Fractional Calculus: Theory and Applications of Differentiation and Integration to Arbitrary Order*. Academic Press; 1974.
- [25] Lovoie JL, Osler TJ, Tremblay R. Fractional derivatives and special functions. *SIAM Rev.* 1976;18:240-268.
- [26] Kilbas A, Srivastava HM, Trujillo JJ. *Theory and Applications of Fractional Differential Equations*. Elsevier; 2006.
- [27] Li C, Cai M. *Theory and Numerical Approximations of Fractional Integrals and Derivatives*. SIAM; 2019.
- [28] Caputo M. Linear models of dissipation whose  $Q$  is almost frequency independent-II. *Geophys J Int.* 1967;13:529.
- [29] Uchaikin VV. *Fractional Derivatives for Physicists and Engineers*. Springer; 2013.
- [30] Cai M, Li C. On Riesz derivative. *Fractional Cal Appl Anal.* 2019;22:287-301.
- [31] Mandelbrot BB. *The Fractal Geometry of Nature*. W. H. Freeman; 1982.
- [32] Klein C, Stoilov N. Multidomain spectral approach to rational-order fractional derivatives. *Stud Appl Math.* 2024;152:1110-1132.
- [33] Kivshar YS, Agrawal GP. *Optical Solitons: From Fibers to Photonic Crystals*. Academic Press; 2003.
- [34] Huang C, Deng H, Zhang W, Ye F, Dong L. Fundamental solitons in the nonlinear fractional Schrödinger equation with a  $\mathcal{PT}$ -symmetric potential. *EPL.* 2008;122:24002.
- [35] Huang C, Dong L. Gap solitons in the nonlinear fractional Schrödinger equation with an optical lattice. *Opt Lett.* 2016;41:5636-5639.
- [36] Zhang L, Li C, Zhong H, Xu C, Lei D, Li Y, Fan D. Propagation dynamics of super-Gaussian beams in fractional Schrödinger equation: from linear to nonlinear regimes. *Opt Exp.* 2016;24:14406-14418.
- [37] Yao X, Liu X. Off-site and on-site vortex solitons in space-fractional photonic lattices. *Opt Lett.* 2018;43:5749-5752.
- [38] Chen M, Zeng S, Lu D, Hu W, Guo Q. Optical solitons, self-focusing, and wave collapse in a space-fractional Schrödinger equation with a Kerr-type nonlinearity. *Phys Rev E.* 2018;98:022211.
- [39] Xie J, Zhu X, He Y. Vector solitons in nonlinear fractional Schrödinger equations with parity-time-symmetric optical lattices. *Nonlinear Dyn.* 2019;97:1287.
- [40] Zeng L, Zeng J. Preventing critical collapse of higher-order solitons by tailoring unconventional optical diffraction and nonlinearities. *Commun Phys.* 2020;3:26.
- [41] Qiu Y, Malomed BA, Mihalache D, Zhu X, Peng X, He Y. Stabilization of single- and multi-peak solitons in the fractional nonlinear Schrödinger equation with a trapping potential. *Chaos Solitons & Fractals.* 2020;140:110222.
- [42] Li P, Dai C. Double loops and pitchfork symmetry breaking bifurcations of optical solitons in nonlinear fractional Schrödinger equation with competing cubic-quintic nonlinearities. *Ann Phys.* 2020;532:2000048.
- [43] Kumar S, Li P, Malomed BA. Domain walls in fractional media. *Phys Rev E.* 2022;106:054207.
- [44] Zhong M, Wang L, Li P, Yan Z. Spontaneous symmetry breaking and ghost states supported by the fractional  $\mathcal{PT}$ -symmetric saturable nonlinear Schrödinger equation. *Chaos.* 2023;33:013106.
- [45] Zhong M, Yan Z. Formation of multi-peak gap solitons and stable excitations for double-Lévy-index and mixed fractional NLS equations with optical lattice potentials. *Proc R Soc A.* 2023;479:20230222.
- [46] Zhong M, Yan Z. Spontaneous symmetry breaking and ghost states in two-dimensional fractional nonlinear media with non-Hermitian potential. *Commun Phys.* 2023;6:92.
- [47] Zhong M, Chen Y, Yan Z, Malomed BA. Suppression of soliton collapses, modulational instability and rogue-wave excitation in two-Lévy-index fractional Kerr media. *Proc R Soc A.* 2024;480:20230765.
- [48] Zangmo T, Mayteevarunyoo T, Malomed BA. Interactions between fractional solitons in bimodal fiber cavities. *Stud Appl Math.* 2024;e12706.

- [49] Feng Z, Su Y. Ground state solutions of fractional equations with Coulomb potential and critical exponent. *Stud Appl Math.* 2024;e127236.
- [50] Malomed BA. Optical solitons and vortices in fractional media: A mini-review of recent results. *Photonics.* 2021;8:353.
- [51] Malomed BA. Basic fractional nonlinear-wave models and solitons. *Chaos.* 2024;34:022102.
- [52] Kevrekidis PG, Cuevas-Maraver J, eds. *Fractional Dispersive Models and Applications: Recent Developments and Future Perspectives.* Springer;2024.
- [53] Li P, Sakaguchi H, Zeng L, Zhu X, Mihalache D, Malomed BA. Second-harmonic generation in the system with fractional diffraction. *Chaos, Solitons & Fractals.* 2023;173:113701.
- [54] Ciaurri O, Roncal L, Stinga PR, Torrea JL, Varona JL. Nonlocal discrete diffusion equations and the fractional discrete Laplacian, regularity and applications. *Adv Math.* 2018;330:688-738.
- [55] Molina MI. The fractional discrete nonlinear Schrödinger equation. *Phys Lett A.* 2020;384:126180.
- [56] Molina MI. The two-dimensional fractional discrete nonlinear Schrödinger equation. *Phys Lett A.* 2020;384:126835.
- [57] Molina MI. Fractional nonlinear electrical lattice. *Phys Rev E.* 2021;104:024219.
- [58] Molina MI. Fractionality and  $\mathcal{PT}$  symmetry in a square lattice. *Phys Rev A.* 2022;106:L040202.
- [59] Kirkpatrick K, Lenzmann E, Staffilani G. On the continuum limit for discrete NLS with long-range lattice interactions. *Commun Math Phys.* 2013;317:563-591.
- [60] Gaididei YB, Mingaleev SF, Christiansen PL, Rasmussen K. Effects of nonlocal dispersive interactions on self-trapping excitations. *Phys Rev E.* 1997;55:6141.
- [61] Jenkinson M, Weinstein MI. Discrete solitary waves in systems with nonlocal interactions and the Peierls-Nabarro barrier. *Commun Math Phys.* 2017;351:45-94.
- [62] Zhong M, Malomed BA, Yan Z. Dynamics of discrete solitons in the fractional discrete nonlinear Schrödinger equation with the quasi-Riesz derivative. *Phys Rev E.* 2024;110:014215.
- [63] Benjamin TB, Feir JE. The disintegration of wave trains on deep water part 1. *J Fluid Mech.* 1967;27:417.
- [64] Christodoulides, DN, Joseph, RI. Discrete self-focusing in nonlinear arrays of coupled waveguides. *Opt Lett.* 1998;13,794-796.
- [65] Kivshar YS, Peyrard M. Modulational instabilities in discrete lattices. *Phys Rev A.* 1992;46,3198.
- [66] Zakharov VE, Ostrovsky LA. Modulation instability: The beginning. *Physica D.* 2009;238:540-548.
- [67] Whitham GB. Non-linear dispersive waves. *Proc R Soc A.* 1965;283,238-261.
- [68] Bespalov VI, Talanov VI. Filamentary structure of light beams in nonlinear liquids. *Sov Phys JETP.* 1966;3:307.
- [69] Ostrovskii LA. Propagation of wave packets and space-time self-focusing in a nonlinear medium. *Sov Phys JETP.* 1967;24,797-800.
- [70] Taniuti T, Washimi H. Self-trapping and instability of hydromagnetic waves along the magnetic field in a cold plasma. *Phys Rev Lett.* 1968;21,209.
- [71] Hasegawa A. Observation of self-trapping instability of a plasma cyclotron wave in a computer experiment. *Phys Rev Lett.* 1970;24,1165.
- [72] Solli DR, Ropers C, Koonath P, Jalali B. Optical rogue waves. *Nature.* 2007;450:1054.
- [73] Chan NN, Chow KW, Kedziora DJ, Grimshaw RHJ, Ding E. Rogue wave modes for a derivative nonlinear Schrödinger model. *Phys Rev E* 2014;89:03294.
- [74] Draper L. Freak ocean waves. *Oceanus.* 1964;10:13-15.

- [75] Chabchoub A, Hoffmann NP, Akhmediev N. Rogue wave observation in a water wave tank. *Phys Rev Lett*. 2011;106:204502.
- [76] Ganshin AN, Efimov VB, Kolmakov GV, Mezhev-Deglin LP, McClintock PVE. Observation of an inverse energy cascade in developed acoustic turbulence in superfluid Helium. *Phys Rev Lett*. 2008;101:065303.
- [77] Bailung H, Sharma SK, Nakamura Y. Observation of Peregrine solitons in a multicomponent plasma with negative ions. *Phys Rev Lett*. 2011;107:255005.
- [78] Bludov YV, Konotop VV, Akhmediev N. Matter rogue waves. *Phys Rev A*. 2009;80:033610.
- [79] Yan Z, Konotop VV, Akhmediev N. Three-dimensional rogue waves in nonstationary parabolic potentials. *Phys Rev A*. 2010;82:036610.
- [80] Iafrati A, Babanin A, Onorato M. Modulational instability, wave breaking, and formation of large-scale dipoles in the atmosphere. *Phys Rev Lett*. 2013;110:184504.
- [81] Yan Z. Financial rogue waves. *Commun Theor Phys*. 2010;54:947.
- [82] Yan Z. Vector financial rogue waves. *Phys Lett A*. 2011;375:4274.
- [83] Akhmediev N, Ankiewicz A, Taki M. Waves that appear from nowhere and disappear without a trace. *Phys Lett A*. 2009;373:675-678.
- [84] Peregrine DH. Water waves, nonlinear Schrödinger equations and their solutions. *J Aust Math Soc B*. 1983;25:16.
- [85] Kibler B, Fatome J, Finot C, Millot G, Dias F, Genty G, Akhmediev N, Dudley JM. The Peregrine soliton in nonlinear fibre optics. *Nat Phys*. 2010;6:790.
- [86] Kharif C, Pelinovsky EN, Physical mechanisms of the rogue wave phenomenon. *Euro J Mech-B/Fluids*. 2003; 22:603-634.
- [87] Onorato M, Residori S, Bortolozzo U, Montina A, Arecchi FT. Rogue waves and their generating mechanisms in different physical contexts. *Phys Rep*. 2013; 528: 47.
- [88] Guo B, Tian L, Yan Z, Ling L, Wang YF. *Rogue waves: mathematical theory and applications in physics*. De Gruyter; 2017.
- [89] Dudley JM, Genty G, Mussot A, Chabchoub A, Dias F. Rogue waves and analogies in optics and oceanography. *Nat Rev Phys*. 2019; 1:675-689.
- [90] Slunyaev AV, Pelinovsky DE, Pelinovsky EN. Rogue waves in the sea: observations, physics, and mathematics. *Phys Usp*. 2023; 66:148-172.
- [91] Ankiewicz A, Akhmediev N, Soto-Crespo JM. Discrete rogue waves of the Ablowitz-Ladik and Hirota equations. *Phys Rev E*. 2010;82:026602.
- [92] Ankiewicz A, Devine N, Ünal M, Chowdury A, Akhmediev N. Rogue waves and other solutions of single and coupled Ablowitz-Ladik and nonlinear Schrödinger equations. *J Opt*. 2013;15:064008.
- [93] Yan Z, Jiang D. Nonautonomous discrete rogue wave solutions and interactions in an inhomogeneous lattice with varying coefficients. *J Math Anal Appl*. 2012; 395: 542-549.
- [94] Ohta Y, Yang JK. General rogue waves in the focusing and defocusing Ablowitz-Ladik equations. *J Phys A*. 2014;47:255201.
- [95] Wen XY, Yan Z. Modulational instability and dynamics of multi-rogue wave solutions for the discrete Ablowitz-Ladik equation. *J Math Phys*. 2018;59:073511.
- [96] Feng BF, Ling L, Zhu ZN. A focusing and defocusing semi-discrete complex short pulse equation and its various soliton solutions. *Proc R Soc A*. 2021;477:20200853.
- [97] Chowdury A, Ankiewicz A, Akhmediev N. Solutions of the higher-order Manakov-type continuous and discrete equations. *Phys Rev E*. 2014;90:012902.

- [98] Wen XY, Yan Z, Malomed BA. Higher-order vector discrete rogue-wave states in the coupled Ablowitz-Ladik equations: Exact solutions and stability. *Chaos*. 2016;26:123110.
- [99] Chen J, Pelinovsky DE. Rogue waves arising on the standing periodic waves in the Ablowitz-Ladik equation. *Stud Appl Math*. 2024;152:147-173.
- [100] Lederer F, Stegeman GI, Christodoulides DN, Assanto G, Segev M, Silberberg Y. Discrete solitons in optics. *Phys Rep*. 2008;463:1-126.
- [101] Kevrekidis PG. *The discrete nonlinear Schrödinger equation: mathematical analysis, numerical computations and physical perspectives*. Springer;2009.
- [102] Kevrekidis PG, Rasmussen KO, Bishop AR. The discrete nonlinear Schrödinger equation: A survey of recent results. *Int J Mod Phys B*. 2001;15:2833.
- [103] Kowalski K, Rembielinski J. Relativistic massless harmonic oscillator. *Phys Rev A*. 2010;81:012118.
- [104] Lörinczi J, Malecki J. Spectral properties of the massless relativistic harmonic oscillator. *J Diff Equ*. 2012;253:2846.
- [105] Pelinovsky DE, Kevrekidis PG, Frantzeskakis DJ. Persistence and stability of discrete vortices in nonlinear Schrödinger lattices. *Physica D*. 2005;212:20-53.
- [106] Bertola M, Tovbis A. Asymptotics of the rational solutions to the focusing nonlinear Schrödinger equation. *Commun Pure Appl Math*. 2013;66:678.
- [107] Tikan A, Billet C, El G, Tovbis A, Bertola M, Sylvestre T, Gustave F, Randoux S, Genty G, Suret P, Dudley JM. Experimental observation of Peregrine solitons in a nonlinear fiber. *Phys Rev Lett*. 2017;119:033901.
- [108] Charalampidis EG, Cuevas-Maraver J, Frantzeskakis DJ, Kevrekidis PG. Rogue waves in ultracold bosonic seas. *Rom Rep Phys*. 2018;70:504.
- [109] Höhmann R., Kuhl U., Stöckmann HJ, Kaplan L, Heller EJ. Observation of Anderson localization in microwave billiards. *Phys Rev Lett*. 2010;104:093901.
- [110] Pelinovsky DE, Kevrekidis PG, Frantzeskakis DJ. Stability of discrete solitons in nonlinear Schrödinger lattices. *Physica D*. 2005;212:1-19.
- [111] Atkinson K. *An Introduction to Numerical Analysis*. John Wiley & Sons; 1991.
- [112] MacKay RS, Aubry S. Proof of existence of breathers for time-reversible or Hamiltonian networks of weakly coupled oscillators. *Nonlinearity*. 1994;7:1623.
- [113] Klein C, Sparber C, Markowich PA. Numerical study of fractional nonlinear Schrödinger equations. *Proc R Soc A*. 2014;470:20140364.
- [114] Frank RL, Lenzmann E. Uniqueness of non-linear ground states for fractional Laplacians in  $\mathbb{R}$ . *Acta Math*. 2013;210:261-318.
- [115] Malomed BA, Kevrekidis PG. Discrete vortex solitons. *Phys Rev E*. 2001;64:026601.
- [116] Zhang X, Xu X, Zheng Y, Chen Z, Liu B, Huang C, Malomed BA, Li Y. Semidiscrete quantum droplets and vortices. *Phys Rev Lett*. 2019;123:133901.